Scilight

Materials Matter

https://www.sciltp.com/journals/mm

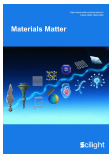

Review

A Brief Overview of Air-Processed Polycrystalline Perovskite Light-Emitting Diodes

Xi Chen †, Eng Liang Lim *,† and Zhanhua Wei *

Xiamen Key Laboratory of Optoelectronic Materials and Advanced Manufacturing, Institute of Luminescent Materials and Information Displays, College of Materials Science and Engineering, Huaqiao University, Xiamen 361021, China

* Correspondence: limengliang1987@hqu.edu.cn (E.L.L.); weizhanhua@hqu.edu.cn (Z.W.)

† These authors contributed equally to this work.

How To Cite: Chen, X.; Lim, E.L.; Wei, Z.; A Brief Overview of Air-Processed Polycrystalline Perovskite Light-Emitting Diodes. *Materials Matter* **2026**, *1*(1), 3.

Received: 13 April 2026

Revised: 26 May 2026

Accepted: 2 June 2026

Published: 16 June 2026

Abstract: Perovskite light-emitting diodes (PeLEDs) have attracted tremendous attention owing to their exceptional luminescent properties. Through extensive research efforts, the external quantum efficiency of fabricated PeLEDs under controlled environments has reached 42.9%. Nevertheless, the realization of high-performance and stable PeLEDs fabricated in ambient air is critically important, as it offers reduced manufacturing costs and compatibility with large-area fabrication processes. However, the primary challenge of air-processed PeLEDs lies in humidity-induced degradation and altered crystallization kinetics, leading to increased defect density and phase transitions within the perovskite films during the deposition process. In this review, we explore the impact of ambient moisture on perovskite films while highlighting recent strategies for optimizing air-processed PeLEDs through additive engineering, antisolvent engineering, and interface engineering. Furthermore, we discuss the remaining challenges associated with air-processed PeLEDs and outline future research directions for scalable and reliable manufacturing, aiming to guide the development of high-efficiency PeLEDs with superior stability.

Keywords: ambient-air; moisture; perovskite light-emitting diodes; crystallization regulation; polycrystalline perovskite

1. Introduction

Perovskite light-emitting diodes (PeLEDs) are considered as a highly promising candidate for the next-generation display and lighting technology due to their tunable spectral characteristics, high color purity display, and low-cost manufacturing process [1,2]. However, the inherent sensitivity of perovskite emitters to moisture and oxygen makes processing them in ambient air particularly challenging. Exposure of perovskite emitter to air can induce rapid phase degradation, increase defect density, and promote non-radiative recombination pathways, ultimately leading to deteriorated optical and device performance [3–5]. Currently, high-performance PeLEDs reported in the literature rely on fabrication within controlled inert environments (i.e., nitrogen-filled glove boxes) featuring extremely low concentrations of humidity and oxygen. Under these conditions, degradation and defect formation during perovskite thin film deposition are effectively suppressed [6,7]. Combined with device engineering, this has resulted in high external quantum efficiency (EQE) of 42.9% [8], 32.5% [9], and 26.4% [10] for green, red and blue-based PeLEDs, respectively, comparable to those achieved by mature technologies like organic light-emitting diodes [8,11,12].

In contrast, the development of air-processed PeLEDs has received comparatively less attention than their inert-atmosphere-processed counterparts, largely due to historically lower efficiencies and limited operational lifespans [13–15]. Recently, however, researchers have developed approaches leveraging perovskite

crystallization regulation [16,17] and interface engineering [18,19] to tackle the challenges posed by air-processed PeLEDs. Benefitting from these approaches, the performance and stability gap between air-processed and inert-atmosphere-fabricated devices has been substantially narrowed [20]. More intriguingly, studies have demonstrated that exposure of the perovskite emitters to moisture helps to passivate defects, alter crystallization kinetics, improve interfacial energy alignment, and thereby enhance radiation recombination efficiency [21,22]. These advancements demonstrate that ambient-air processing is not merely a cost-motivated compromise, but a promising manufacturing approach with distinct potential advantages, such as accelerating their transition from laboratory-scale demonstrations toward large-area and flexible optoelectronic systems. Although perovskite quantum dots exhibit distinct surface-ligand-stabilized architectures and have shown promising ambient stability, their degradation mechanisms and processing chemistry differ fundamentally from those of polycrystalline thin films. Therefore, this review focuses specifically on polycrystalline PeLEDs, in which grain-boundary-dominated instability poses unique challenges under ambient-air fabrication. We first provide a concise analysis of the degradation mechanisms of metal halide perovskites (MHPs) induced by moisture. We then summarize the recent progress in the fabrication of PeLEDs under ambient-air conditions. Finally, we discuss the remaining challenges associated with air-processed PeLEDs and outline future research directions toward scalable and reliable manufacturing, aiming to guide the development of high efficiency PeLEDs with superior stability.

2. The Crystal Structure of Polycrystalline Metal Halide Perovskite

For perovskite emitters used in LED application, these materials can be categorized into three-dimensional (3D) or quasi-two-dimensional (quasi-2D) crystal structures. The 3D structure typically has the chemical formula of ABX_3 (A = MA^+, FA^+ or Cs^+, B = Pb^{2+} or Sn^{2+}, and X = I^-, Br^- or Cl^-). By cutting the typical 3D MHP (Figure 1a) consisting of corner-sharing lead halide octahedra along (100), (110), and (111) directions (Figure 1b) and inserting a bulky organic spacer cation, a new structural and compositional dimension is formed, with the chemical formula of $A'_mA_{n-1}B_nX_{3n+1}$. Here, the monovalent (m = 2) or divalent (m = 1) bulky spacer cation can intercalate between the anions of the 2D perovskite sheets, where n represents the number of inorganic octahedral sheets sandwiched between two organic interlayers. The 2D and quasi-2D perovskites are obtained when one octahedral layer (n =1) and n octahedral layers (n >1) are separated by the organic spacer cations, respectively. Compared with the 2D MHP, obtaining a truly pure n-value quasi-2D film is challenging due to the different formation energy of the multiple quantum wells with different n values, which self-assemble in a bottom-up manner. Through chemical dimensionality manipulation of 3D MHP, three types of low-dimensional perovskites can be obtained (Figure 1c): (i) Dion–Jacobson (DJ) perovskite with the chemical formula of $A'A_{n-1}B_nX_{3n+1}$, (ii) Ruddlesden–Popper (RP) perovskite with the chemical formula of $A'_2A_{n-1}B_nX_{3n+1}$ and (iii) alternating cation in the interlayer space (ACI) with the chemical formula of $A'A_nB_nX_{3n+1}$. For an ACI low dimensional perovskite, the A-site 'perovskitizer' (MA^+, FA^+, or Cs^+) not only resides in the perovskite slab, but also occupies the interlayer along with the specified spacing cation. It usually involve acetamidinium (ACA^+) [23] or guanidinium (GA^+) [24] as the interlayer cation.

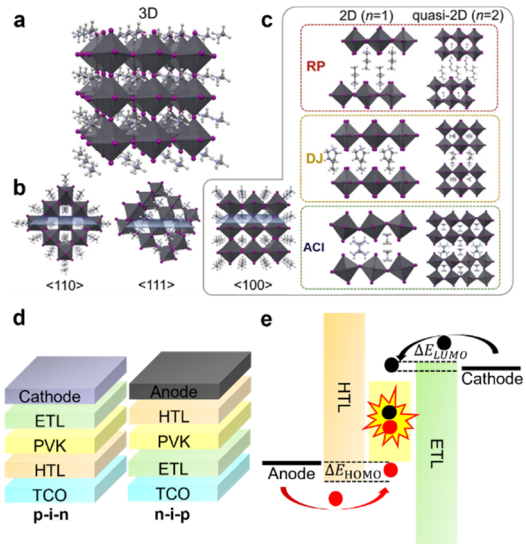

Figure 1. (**a**) 3D perovskite crystal structure. (**b**) The bulky organic spacer cation slices the n layers of corner-sharing lead halide octahedra along <100>, <111>, and <100> directions. (**c**) The 2D (n = 1) and the quasi-2D

perovskite crystal structure (n = 2) of RP, DJ and ACI along <100> direction. Reproduced with permission [25]. Copyright 2022, Springer Nature. (**d**) Architecture of PeLED: (**left**) conventional and (**right**) inverted structures. (**e**) Working mechanism of a PeLED.

3. Working Principle of PeLED

PeLEDs feature a conventional sandwich structure, whereby the perovskite light-emission layer (LEL) is sandwiched between the p-type and n-type charge transport layers (CTLs). Such a configuration is crucial for device applications, as it promotes carrier injection and transport, confines the recombination region, suppresses non-radiative interfacial recombination, and enhances operational stability. Depending on the stacking order of the CTLs, the architecture of PeLED can be divided into two main types: the conventional (p-i-n) structure and the inverted (n-i-p) structure, as shown in Figure 1d. As an electroluminescent device, under the action of an applied electric field, electrons and holes are injected from the cathode and anode, respectively. Then, these carriers are injected into the conduction band (CB) and valence band (VB) of the perovskite through the lowest unoccupied molecular orbital (LUMO) of the electron transport layer (ETL) and the highest occupied molecular orbital (HOMO) of the hole transport layer (HTL), respectively, ultimately recombining to form excitons or undergoing free carrier recombination within the perovskite LEL, and emitting photons to achieve electroluminescence (EL). Therefore, several conditions are required to realize efficient EL: (1) efficient carrier injection, that is, energy loss (ΔE_{LUMO} and ΔE_{HOMO}) during the injection of electrons and holes from the electrode to the perovskite should be minimized (Figure 1e); (2) balanced carrier injection, that is, the ratio of electrons and holes reaching the LEL should approach unity; (3) recombination should be confined within the LEL, and leakage currents into adjacent transport layers should be avoided; (4) the ratio of radiative recombination to non-radiative recombination should be maximized; and (5) effective light extraction, that is, the proportion of photons generated by the LEL escaping from the device should be maximized. Accordingly, the EQE of the PeLEDs can be described by Equation (1):

$$EQE = f_{\text{balance}} \times f_{\text{e-h}} \times \eta_{\text{rad}} \times f_{\text{outcoupling}} \quad (1)$$

where f_{balance} represents the probability of balanced charge injection, with a maximum value equal to 1, $f_{\text{e-h}}$ is the probability of forming a correlated electron–hole pair or exciton from each pair of injected carriers, η_{rad} is the probability of radiative recombination for the exciton or electron–hole pair and $f_{\text{outcoupling}}$ is the optical outcoupling efficiency [26].

4. Insights into Perovskite-Water Interactions

The inherent ionic and soft lattice nature of MHPs renders them highly susceptible to polar water molecules. This sensitivity arises from the ability of water molecules to form hydrogen bonds with electronegative species bearing lone electron pairs, such as the nitrogen atoms in organic cations and the halogen anions [6]. In addition, water can coordinate with under-coordinated Pb^{2+} centers, further destabilizing the octahedral framework. These interactions disrupt the perovskite lattice and may ultimately trigger hydrate formation, phase transitions, decomposition, and eventual dissolution [27–29]. Therefore, elucidating the mechanisms of perovskite-water interactions is crucial for the development of air-based processed PeLEDs.

4.1. 3D Perovskite

Depending on the type of A-site cation, MHPs undergo distinct chemical processes upon exposure to trace amounts of water (Figure 2a). For example, for organic–inorganic hybrid perovskites containing NH_3^+-functionalized cations (e.g., $MAPbX_3$, $FAPbX_3$), water molecules can form hydrogen bonds with the organic species, leading to the formation of hydrated intermediates such as monohydrate ($APbX_3 \cdot H_2O$) and dihydrate ($A_4PbX_6 \cdot 2H_2O$). In the case of $MAPbI_3$, these intermediates subsequently decompose into PbI_2 and organic byproducts (Equation (2)) [29]. Interestingly, the monohydrate $CH_3NH_3PbI_3 \cdot H_2O$ can still be restored upon drying. Once the dihydrate $(CH_3NH_3)_4PbI_6 \cdot 2H_2O$ forms—accompanied by the generation of PbI_2—the restoration becomes incomplete, leading to performance degradation of the devices. When exposed to excessive water, $CH_3NH_3PbI_3$ undergoes a complete hydrolysis (Equation (3)). In this process, the organic cations are protonated and subsequently released in gaseous or dissolved form, with PbI_2 precipitating as a solid residue. Meanwhile, it has also been reported that water exposure induces phase transition in inorganic halide perovskites. Owing to the high solubility of CsBr (up to 1243 g/L at 25 °C), preferential loss of the CsBr component from $CsPbBr_3$ occurs, which leads to the formation of the CsBr-deficient $CsPb_2Br_5$ phase. In contrast, for zero-dimensional Cs_4PbBr_6 perovskite with a higher CsBr content, water triggers a phase transition toward $CsPbBr_3$ [27]. This hydration process can be reversed under appropriate conditions by removing water. Under exposure to high water

concentrations, the mixed halide perovskite $Cs_{0.05}(MA_{0.17}FA_{0.83})_{0.95}Pb(Br_{0.17}I_{0.83})_3$ (CsMAFA) undergoes pronounced spinodal decomposition (Figure 2b) [28]. In this process, interaction with water dissolves the organic constituent of nanoscale CsMAFA, initiating spontaneous phase separation into PbI_2 and $CsPb_2Br_5$. At this intermediate stage, CsMAFA, PbI_2, and $CsPb_2Br_5$ coexist within individual particles. The dissolution-recrystallization mechanism governing the transformation from CsMAFA to PbI_2 and $CsPb_2Br_5$ either competes with or follows the initial decomposition process, which ultimately dictating the final particle morphology—resulting in a mixture of small polygonal and needle-like features. Continued water exposure promotes further degradation, resulting in dissolution of $CsPb_2Br_5$ and complete decomposition of PbI_2.

$$4CH_3NH_3PbI_3 + 4H_2O \rightarrow 4[CH_3NH_3PbI_3 \cdot H_2O] \rightarrow (CH_3NH_3)_4PbI_6 \cdot 2H_2O + 3PbI_2 + 2H_2O \quad (2)$$

$$CH_3NH_3PbI_3 + H_2O \rightarrow PbI_2 + CH_3NH_2 + HI \quad (3)$$

Basically, perovskite does not simply dissociate into A^+, Pb^{2+}, and X^- ions in water. Instead, Pb^{2+} readily coordinates with excess halide ions to form haloplumbate complexes (e.g., $[PbI_4]^{2-}$, $[PbBr_4]^{2-}$), which significantly increase the apparent solubility of the perovskite [30]. The complexation equilibrium in perovskite is therefore highly sensitive to the halide ion concentration and the solution pH. In the presence of excess X^-, the equilibrium is shifted toward higher-coordination haloplumbate species, suppressing the precipitation of PbX_2 and, in some cases, promoting the redissolution of previously formed decomposition products [30,31]. This property is utilized in aqueous-phase synthesis of nanocrystals, but it also implies that perovskites are highly susceptible to leaching in water environments [32]. Given the inherent instability of 3D perovskites toward water, researchers are compelled to develop new strategies and explore alternative research directions to enhance their water tolerance.

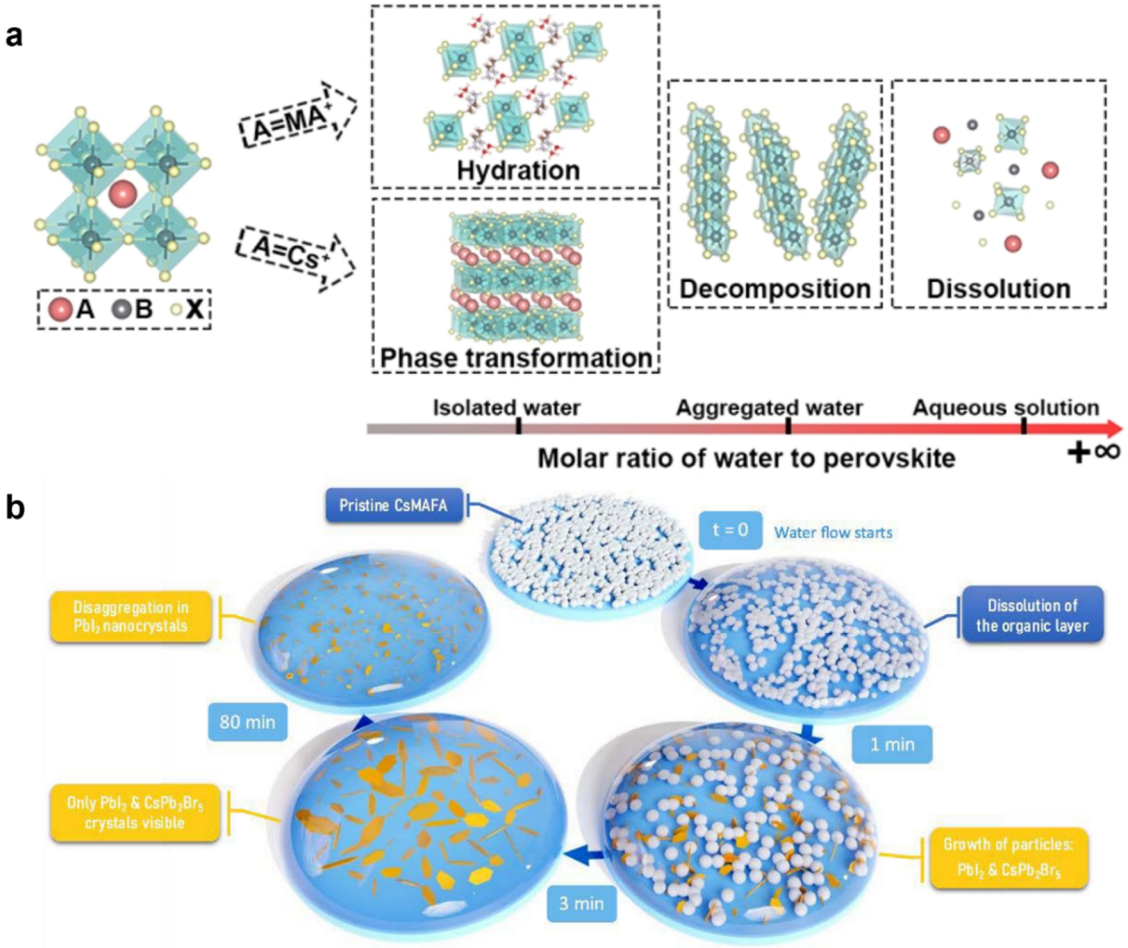

Figure 2. (**a**) Schematic illustration of perovskite-water interactions. Reproduced with permission [27]. Copyright 2020, American Chemical Society. (**b**) Reaction scheme and observations of CsMAFA in water. Reproduced with permission [28]. Copyright 2024, Royal Society of Chemistry.

4.2. Quasi-2D Perovskite

In humid environments, quasi-2D perovskites are known to exhibit superior stability relative to their 3D counterparts. This enhanced stability is attributed to the incorporation of organic spacer cations, which feature hydrophobic alkyl/aryl hydrocarbon chains alongside hydrophilic amino groups. In terms of spatial structure, the hydrocarbon chains of the quasi-2D perovskites tend to self-assemble, forming a hydrophobic surface that serves as a physical barrier to hinder the ingression of water molecules. Concurrently, ion migration (e.g., I^-, MA^+) within the perovskite is substantially suppressed, which in turn mitigates defect formation and ion escape processes that would otherwise be exacerbated by water molecules [33]. Using n-butylammonium methylammonium lead iodide (nBA-$MAPbI_3$) as a model system, Wygant et al. [34] proposed that a water-induced disproportionation reaction was a key mechanism governing the water stability of quasi-2D RP perovskites. Upon exposure to water, the quasi-2D perovskite containing higher-n phases undergo a surface transformation into both lower-n and higher-n phases. The formation of more stable lower-n phases on the surface protects the underlying bulk perovskite, thereby enhancing the overall film's tolerance to water. In contrast to the RP phase, the DJ phase features monolayer diamine cations that form hydrogen bonds with the inorganic layers on both sides. This structural configuration leads to a smaller interlayer spacing and stronger interlayer coupling, which is favorable for enhanced stability upon exposure to water. Such a difference in air-moisture stability (or water stability) between quasi 2D RP and DJ perovskites can be attributed to the formation of a distinct van der Waals (vdW) gap in RP phases, where two organic cation layers (e.g., monoammonium based organic molecules) separate adjacent perovskite slabs and interact only via weak vdW forces. In contrast, no vdW gap exists in DJ perovskites because the interlayer region is fully occupied by a bridging cation (e.g., divalent organic cation). For these reasons, water molecules can easily insert into the vdW gap of RP phases and disrupt the weak vdW interactions, creating low energy pathways for water intercalation, which leads to rapid swelling and degradation. Conversely, the absence of a vdW gap and the smaller interlayer spacing in DJ phases effectively block water intercalation, thereby requiring much higher energy for water insertion and offering superior moisture resistance [35,36]. However, recently studies demonstrated that DJ-phase perovskites, such as (PDMA)PbI_4, undergo a distinctly different process—hydration. Water molecules can directly intercalate into the perovskite lattice and disrupt the layered structure, forming a one-dimensional (1D) chain-like hydrate of (PDMA)$Pb_2I_6 \cdot 2H_2O$. The as-formed 1D structure lacks the excellent optoelectronic properties characteristic of quasi-2D materials [37]. Although the hydration process is thermally reversible, it results in a permanent reduction in the crystallinity of the perovskite.

Ab initio molecular dynamics (AIMD) simulations conducted under aqueous environment reveal distinct behaviors for different surface terminations of RP-phase (BA_2PbI_4) and DJ-phase ((3AMP)PbI_4). For the PbI_2-terminated surface, water molecules primarily form Pb–O bonds with surface Pb atoms. The Pb–O interaction is stronger in the RP phase (BA) than in the DJ phase (3AMP), indicating a more pronounced initial reaction of the RP phase with water. For the I-terminated surface, water molecules attack Pb–I bonds, leading to bond breakage, while surface I^- ions undergo oxidation to form I_2 molecules that are subsequently released. This termination exhibits high instability, with such degradation pathways observed in both RP and DJ phases. In contrast, the organic-cation-terminated surface demonstrates the highest stability, as the hydrophobic nature of the organic layer effectively prevents water molecules from penetrating into the inorganic layer [38]. Therefore, the stability of quasi-2D perovskites upon exposure to water is critically governed by their crystal structure, the chemical properties of the organic cations, and the surface termination phase. By rationally designing spacer cations that are incapable of forming stable hydrates, the degradation pathway associated with water incorporation can be effectively mitigated, thereby enhancing the water resistance of quasi-2D perovskite materials.

5. Insights into Perovskite-Oxygen Interactions

According to previous study, the interaction between oxygen and perovskite materials can be categorized into four stages, namely surface adsorption, surface reaction, reactive oxygen species (ROS) diffusion, and bulk reaction. Initially, oxygen is physically adsorbed onto the perovskite surface via van der Waals forces. Under certain conditions, the surface reaction generates ROS, which then diffuse into the bulk perovskite to induce bulk reactions. Notably, the extent and nature of these interactions strongly depend on the generation of ROS [39]. Under dark conditions, the absence of energy-driven electron transfer renders the influence of oxygen on perovskite materials negligible, manifesting primarily as reversible physical adsorption [40]. Nevertheless, it has a significant impact on the electronic structure of the perovskites. For example, the Fermi level of mixed-cation perovskite films has been observed to shift toward the valence band by about 1 eV after exposure to oxygen, indicating oxygen acts as an efficient p-type dopant. This doping effect fully recovers after storage in ultra-high vacuum, demonstrating complete reversibility [41]. Compared with the larger-grain films, smaller-grain films

adsorb more oxygen due to their larger surface area, leading to a more pronounced p-type character upon oxygen exposure [42]. In addition to functioning as a p-type dopant, oxygen also induce defect-healing, in which oxygen adsorption and diffusion mediate the perovskite lattice, passivating various defects such as halide vacancies, interstitials, and halide migration/aggregation [43]. Crucially, moisture and oxygen act synergistically in ambient air. When illuminated, a perovskite releases photogenerated electrons that are rapidly transferred to absorbed oxygen molecules, "activating" them into superoxide radicals (O_2^-). Given their extremely high reactivity, O_2^- serves as the primary precursor for various other ROS [44]. The presence of O_2^- is more destructive than water, as it reacts with the A-site, B-site and X-site ions in the perovskite lattice. Taking $MAPbI_3$ as an example, organic cations undergo deprotonation to form volatile methylamine; Pb^{2+} ions react to form metal oxides, destroying the octahedral structure of the perovskite; and halide ions (e.g., iodide) are oxidized to iodine or oxy-iodide complexes, where iodine triggers a cyclic reaction ($I^- + I_2 \rightleftharpoons I_3^-$), thereby accelerating degradation [39,45–47]. In 2020, Quan et al. reported that charges accumulating at the exposed perovskite edges in reduced-dimensional perovskite can activate physically adsorbed oxygen molecules into reactive superoxide radicals, thereby triggering perovskite degradation [48].

6. Device Engineering Approaches for Air-Processed PeLEDs

To overcome the intrinsic instability and poor crystallization controllability of perovskite films fabricated under ambient air conditions, extensive efforts have been devoted to regulating both the intrinsic composition and the crystallization kinetics of air-processed perovskites. In particular, additive engineering enables the modification of electronic structure and lattice stability at the compositional level, while antisolvent engineering provides an effective route to kinetically control nucleation and crystal growth during film formation. Together, these two strategies play complementary roles in suppressing phase aggregation, reducing defect density, and enhancing the optoelectronic performance of air-processed PeLEDs.

6.1. Additive Engineering

Additive engineering has emerged as an effective strategy to regulate crystallization behavior and enhance the environmental tolerance of the air-processed perovskites. In a recent study, Guo et al. [13] proposed an electronic structure engineering approach based on interstitial doping with trivalent metal cations (Sb^{3+} and Ga^{3+}) to prepare air-processed pure-bromide quasi-2D blue perovskite. With this approach, (i) the precipitation of CsBr induced by ambient humidity was mitigated, resulting in a smoother film (Figure 3a), (ii) the formation of higher-n phases was suppressed while the formation energy of the n = 3 phase was promoted, thereby enhancing the stability of the perovskite in ambient air, and (iii) energy transfer from small-n to large-n phases was promoted while electron–phonon coupling within the perovskite films was suppressed, thereby optimizing the light efficiency of both the films and the target devices (Figure 3b). More intriguingly, the local positive electric field generated by trivalent interstitial dopant ions effectively restricted the motion of negatively charged bromine ions through local electrostatic attraction. This impeded migration of bromine ions facilitated the elimination of halogen vacancies, thereby reducing deep trap states within the bandgap. Consequently, the suppression of bromine migration and the associated reduction in defects enhanced the stability of the perovskite lattice under an applied electric field. Benefitting from these, the target device with an EL peak at 468 nm fabricated under 25% relative humidity (RH) yielded an EQE value of 2.05%. Later, a bifunctional molecule of formamidinium trifluoroacetate (FATFA) was introduced into the perovskite precursor to regulate perovskite crystallization under RH of 25–40% (Figure 3c). At an optimal concentration of 15%, (i) TFA^- anions were found to accelerate perovskite crystallization in air, thereby effectively mitigating moisture-induced corrosion of the emissive layer during film formation; and (ii) FA^+ cations could partially substitute Cs^+ ions and incorporate into the perovskite lattice, resulting in a reduced defect density. As a result, radiative recombination of the resultant perovskite film was enhanced, leading to nearly 44% improvement in device performance for the target device (i.e., EQE increased from 11.12% to 16.01%), and an operational T_{50} lifetime of nearly 25 min at an initial brightness of ~900 cd m^{-2} was obtained [17].

On the other hand, Feng et al. [49] developed a calcium ion confinement (CIC) strategy for preparing high-quality perovskite film via in-situ supercrystal formation under 25–40% RH. By incorporating an optimal amount of $CaBr_2$ into the perovskite precursor, the growth of air-processed $CsPbBr_3$ perovskite was suppressed (denoted as TPBC, Figure 3d), in contrast to the control film (denoted as TFB). The authors attributed this suppression to Ca^{2+} acting as inorganic capping ligands that confined the perovskite grain size. Owing to their moisture-sensitivity, Ca^{2+} tended to detach from the surface, exposing the $[PbBr_6]^{4-}$ octahedra and thereby promoting the growth of perovskite nanocrystals. Concurrently, the moisture-induced detachment of $CaBr_2$ ligands facilitated interactions between adjacent nanocrystals through Coulombic forces, leading to the formation of a

perovskite super crystal (Figure 3e,f). With the incorporation of FA^+ ions, the target device achieved a record luminance of 92,995 cd m^{-2} and an EQE of 10% (nearly 125-fold improvement relative to the control device). Without encapsulation, the device exhibited an operational lifetime (T_{50}) of 8.13 h under an initial luminance of 1,000 cd m^{-2}. Meanwhile, Wang et al. [50] used ambient moisture as a reactive component. They found that incorporating diphenylphosphinic chloride (DPPC) and phenylphosphonic dichloride (PPDC) additives into pure-bromide perovskite precursor solutions triggered hydrolysis and released Cl^- ions, which acted as a chlorine source and led to the formation of Br–Cl mixed halide perovskites. Their finding showed that this moisture-assisted chemical transformation provides an alternative route for compositional modulation, enabling blue emission under ambient air conditions (Figure 3g). Furthermore, Guo et al. [51] demonstrated that quantum well encapsulation was achieved within the perovskite film by leveraging the hydrolysis reaction of $SiBr_4$ or $AlBr_3$ with water in DMSO. Through this approach, a hydroxyl-functionalized oxygen-bridged network was generated, which coordinated with perovskite precursor intermediates to promote stoichiometric crystallization, thereby encapsulating and passivating the quantum wells. Benefitting from this, low-n phase components were stabilized and electron–phonon coupling within these phases were suppressed, resulting in enhanced stability of the perovskite films against environmental stressors. Finally, the target device with an EL peak at 468 nm achieved an EQE of 4.02%. More intriguingly, the device maintained a stable emission color after 2160 h of exposure to ambient environment (10–20% RH) and prolonged thermal aging at 70 °C for 92 h.

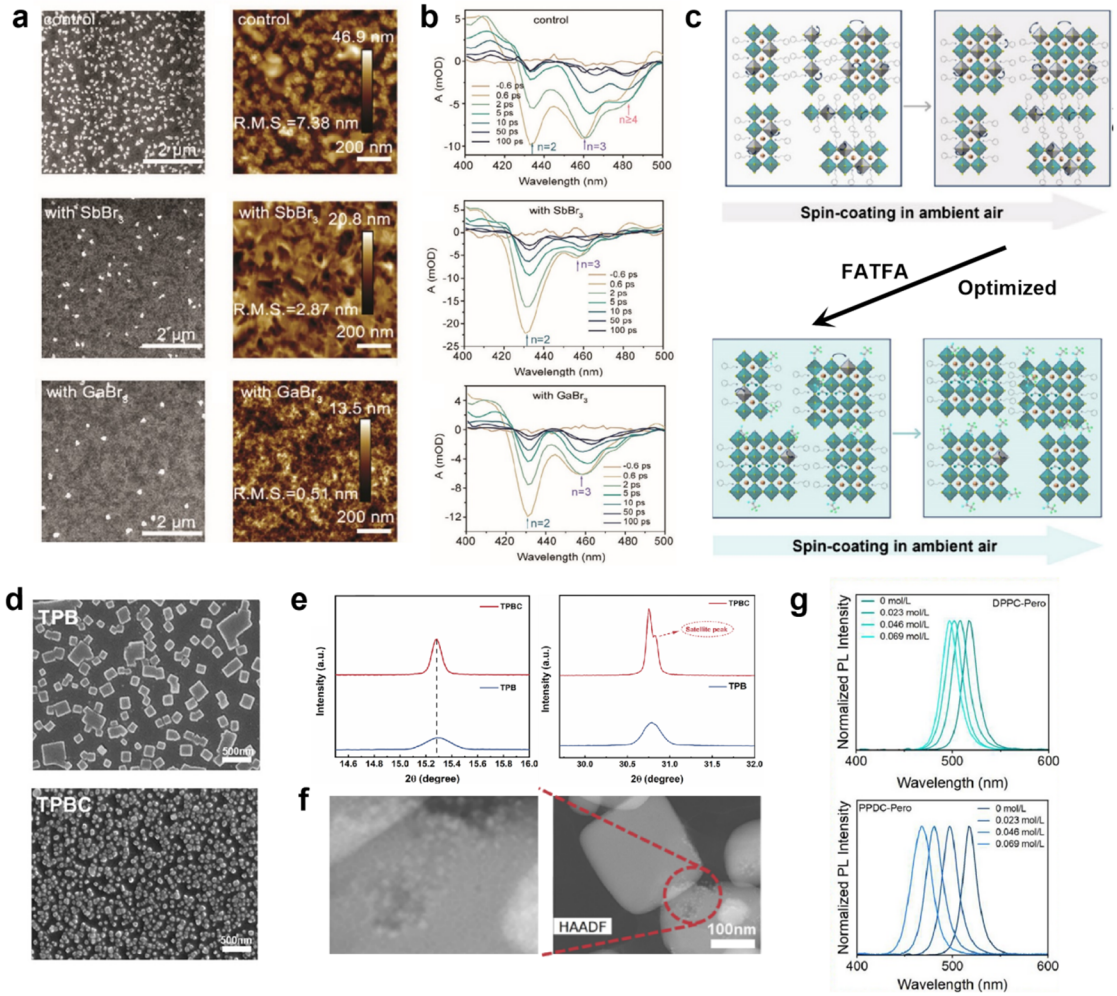

Figure 3. (**a**) SEM images (left), AFM images (right) and (**b**) TAS spectra of the control, $SbBr_3$-treated, and $GaBr_3$-treated perovskite films. Reproduced with permission [13]. Copyright 2025, Wiley-VCH. (**c**) Schematic illustration of crystallization regulation upon the addition of FATFA in quasi-2D $CsPbBr_3$ perovskite. Reproduced with permission [17]. Copyright 2025, American Chemical Society. (**d**) SEM images and (**e**) local magnified XRD patterns of the control (TFB) and Ca^{2+}-treated (TPBC) perovskite films. (**f**) STEM-HAADF image of the Ca^{2+}-treated (TPBC) perovskite films. Reproduced with permission [49]. Copyright 2025, Wiley-VCH GmbH. (**g**) Photoluminescence (PL) spectra comparison of the perovskite films prepared from DPPC (**top**) and PPDC (**bottom**) at different concentrations. Reproduced with permission [50]. Copyright 2024, American Chemical Society.

6.2. Antisolvent Engineering

It is well established that selecting appropriate antisolvents and tailoring the interaction strength with the solvent (DMSO or DMF) is crucial for perovskite film formation, as the antisolvent enables effective regulation of the film growth kinetics, thereby allowing high-quality perovskite films to be prepared in air. Recently, antisolvent engineering using chlorobenzene (PhCl), toluene (PhMe), and diethyl ether (DEE) was implemented to fabricate air-processed quasi-2D PEA–$FAPbBr_3$ perovskites. Among these, DEE exhibited a higher DMSO extraction rate than PhCl and PhMe, which promoted faster nucleation of the perovskite under ambient air conditions (relative humidity of 15–20%). By modulating the nucleation and growth characteristics of the perovskite films through DEE antisolvent, phase aggregation within the quasi-2D perovskite was effectively suppressed. This not only minimizing non-radiative recombination that would otherwise have arisen from charge trapping in aggregated domains during charge transfer within the quasi-2D perovskite, but also led to the formation of a homogeneous film morphology with excellent optoelectronic properties (i.e., uniform photoluminescence intensity and lower trap density, Figure 4a,b). Benefitting from these advantages, excitons transfer efficiency and the radiative recombination within the quasi-2D perovskite were promoted, and the target device treated with DEE achieved an EQE of 15.4% and an operational T_{50} lifetime of nearly 19 min at an initial brightness of 100 cd m^{-2} [3]. Compared with DEE antisolvent, employing n-hexane as the antisolvent reduced the crystallization kinetics of the $Rb_xCs_yPbBr_zCl_{3-z}$ perovskite (prepared from crown, TPPO, DMSO, etc.) owing to the weak interactions between n-hexane and the perovskite. The slower crystallization rate was attributed the presence of these compounds (crown, TPPO, and DMSO) in perovskite precursor, which facilitated the formation of intermediate species that inhibited nucleation and crystallite growth during the perovskite film-forming process. This, in turn, promoted the formation of larger crystal grains with enhanced crystalline quality (as evidenced by a slower change trend in the absorption spectra, Figure 4c) and a lower trap density in the target films (Figure 4d). With these advantages, PL properties of the resulting films were improved. Using this approach, the target device treated with n-hexane achieved an optimal EQE of 5.89% [14].

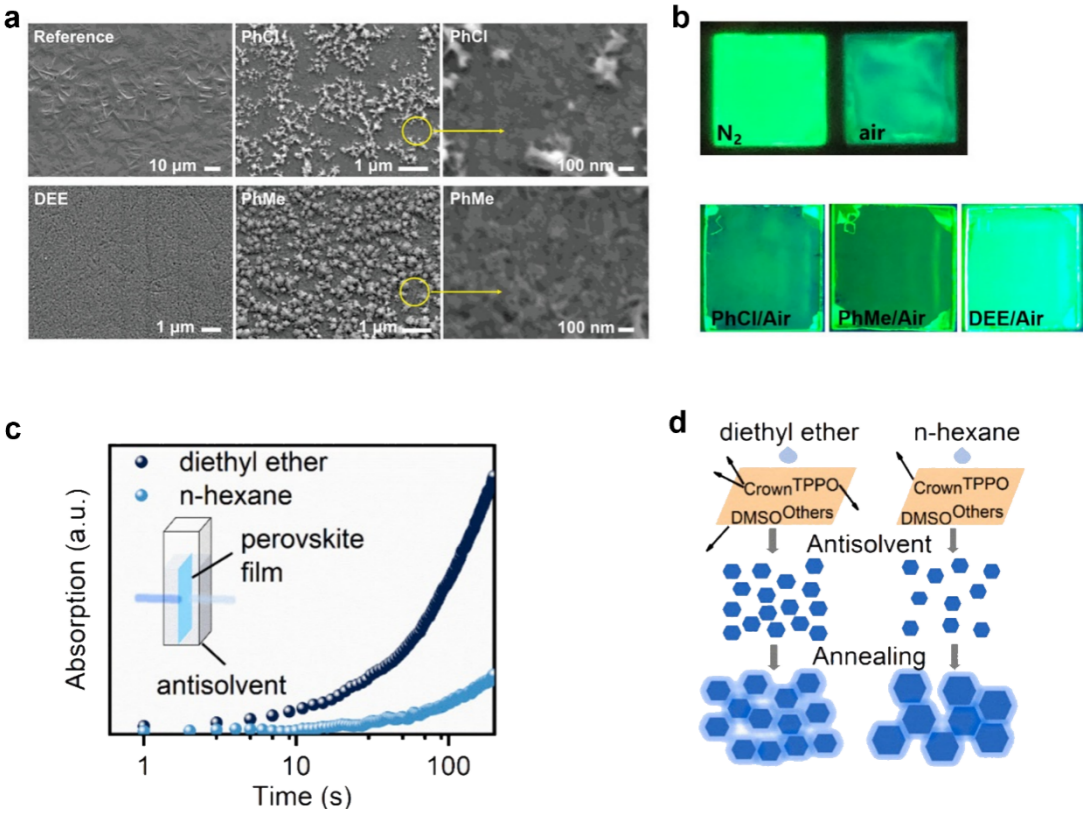

Figure 4. (**a**) SEM images of the perovskite films prior to annealing using PhCl, PhMe and DEE antisolvents. (**b**) Photographs of the perovskite films under 365 nm excitation (**top**) prepared in nitrogen and air condition and (**bottom**) prepared in air condition using PhCl, PhMe and DEE antisolvents. Reproduced with permission [3]. Copyright 2021, WILEY-VCH. (**c**) Time-dependent change in absorption peak intensity at 476 nm of the perovskite films prepared without antisolvent or without thermal treatment immersed in diethyl ether and n-hexane. The inset shows a schematic diagram of the time-dependent absorption measurement method. (**d**) Schematic illustration of

the crystallization mechanism for air-processed perovskite films prepared from diethyl ether and n-hexane as antisolvents. Reproduced with permission [14]. Copyright 2025, Elsevier.

6.3. Interface Engineering

For air-processed PeLEDs, interfaces are required not only to serve their conventional roles in energy level alignment and charge carrier regulation, but also to resist chemical degradation induced by moisture. As the growth template for the perovskite layer, the bottom interface is particularly susceptible to surface chemical evolution upon air exposure. Such water-induced interfacial reconstruction can substantially alter nucleation kinetics and crystallization behavior, thereby determining the initial film quality and morphological uniformity. Therefore, achieving high-efficiency and stable air-processed PeLEDs necessitates deliberate interfacial engineering strategies to systematically regulate interfacial chemistry and structural integrity.

The crystallization kinetics of perovskite films fabricated under ambient air are critically influenced by moisture adsorbed on the substrate. Thus, rational design and modification of the bottom interface have emerged as effective approaches to mitigate moisture-induced degradation and improve film quality. For example, Guo et al. [52] reported that the introduction of perfluorooctanoic acid (PFOA) into PEDOT:PSS reduced its hygroscopicity and effectively modulated the molecular conformation of PEDOT:PSS (Figure 5a), resulting in more ordered PEDOT domains that enhanced charge transport and improved energy level alignment. As a result, the target device fabricated in ambient air achieved a peak EQE of 6.86% (nearly 94% improvement relative to the control device) and a maximum luminance of 854.10 cd m^{-2}. Under high-humidity conditions of 60% RH, Li et al. [53] reported that employing a hydrophobic self-assembled monolayer (SAM) (Figure 5b) as HTL improved perovskite film quality (i.e., higher PLQY, Figure 5c), which helped reduce leakage currents and enhance device performance. Combined with post-treatment using triphenylphosphine oxide (TPPO), radiative recombination in the perovskite film was promoted, while moisture ingress was suppressed, yielding an EQE of 4.87% for the target device (nearly 83% improvement relative to the control device). Meanwhile, the incorporation of poly[(9,9-bis(3′-((N,N-dimethyl)–N-ethylammonium)-propyl)-2,7-fluorene)-alt-2,7-(9,9-dioctylfluorene)] dibromide (PFNBr) at the SAM/perovskite interface eliminated humidity-induced aggregation on the SAM layer, yielding a flatter perovskite film with low surface roughness. In addition to passivating bulk and surface defects, PFNBr also optimized energy level alignment and hole mobility, resulting in balanced charge carrier injection and reduced non-radiative recombination at the HTL/perovskite interface (Figure 5d). As a result, an EQE of 12.06% was achieved for the target device fabricated under 25-40% RH (nearly 63% improvement relative to the control device), with an operational T_{50} of nearly 23 min at an initial brightness of 150 cd m^{-2} [4]. Additionally, Wu et al. [19] incorporated polyethyleneimine sulfonate (PEIS) into NiO_x substrates. They found that the abundant amino and sulfonate groups in PEIS could provide nucleation sites for crystallization regulation, enabling precise control over the crystallization kinetics of different n-phases in air-processed blue perovskite films. Consequently, a peak EQE of 2.34% (nearly 420% improvement relative to the control device) and a maximum luminance of 1161 cd m^{-2} were achieved for the large-area target device. Meanwhile, surface modification of a NiO_x substrate with poly(vinylpyrrolidone) (PVP) was shown to improve the crystallinity of the perovskite emissive layer and effectively reduced defect density. As a result, the target device fabricated in ambient air achieved an EQE of 16.05%, corresponding to a 52% improvement relative to the control device [18].

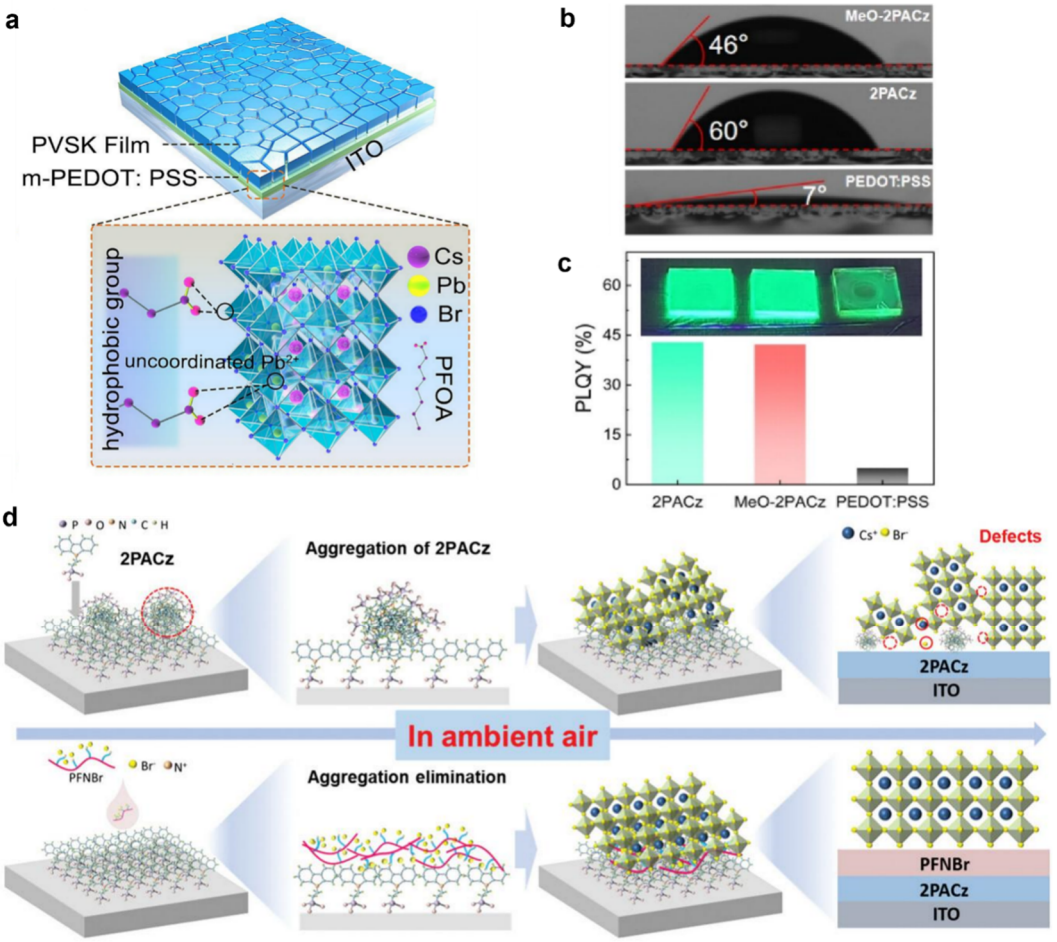

Figure 5. (**a**) Schematic illustration of the coordination interaction between PFOA and perovskite. Reproduced with permission [52]. Copyright 2024, Elsevier. (**b**) water contact angles and (**c**) PLQY measurements of 2PACz, MeO-2PACz and PEDOT:PSS HTLs. Reproduced with permission [53]. Copyright 2023, American Chemical Society. (**d**) Schematic illustration of the coordination interaction between SAM and perovskite layer without and with PFNBr modification in ambient-air environment with 25–40% RH. Reproduced with permission [4]. Copyright 2023, Wiley-VCH GmbH.

7. Conclusions and Future Outlooks

In this brief overview, we have analyzed the degradation mechanisms induced by perovskite–water interactions and summarized recent progress in air-processed PeLEDs (Table 1). Compared with iodide-based perovskites, bromide-based perovskites exhibit improved environmental stability owing to their stronger Pb–Br bonding (248 kJ/mol) [54]. Although chloride-based perovskites may theoretically possess even higher resistance to moisture and oxygen due to their stronger Pb–Cl bond strength (301 kJ/mol) [54], pure chloride-based perovskites usually exhibit wide bandgaps [55], placing their emission wavelengths outside or near the edge of the visible spectrum, which limits their application for air-processed PeLEDs in the visible region. While mixing chloride and bromide can partially tune the bandgap toward the blue spectral region while maintaining visible-light emission [10], this mixed Br–Cl halide introduces new challenges, such as halide phase segregation, increased defect density, spectral instability, and poorer film uniformity arising from the distinct crystallization dynamics and low solubility of chloride precursors [10,56]. These issues further increase the complexity of preparing perovskite films in an air environment. As such, bromide-based perovskites are currently regarded as the main research focus for air-processed PeLEDs because they offer a more favorable balance among visible luminescence performance, environmental stability, and solution processability [13]. Nevertheless, the inherent unpredictability of humidity in real ambient conditions continue to pose significant challenges to film crystallinity and device uniformity. To address these challenges, researchers have employed various strategies (i.e., additive engineering, antisolvent engineering, and interface engineering) to regulate the nucleation and growth of perovskite films, thereby optimizing the performance of air-processed PeLEDs. Based on these advances, we propose several perspectives to guide further development in this field.

(1) Enhancing the intrinsic air stability of perovskite materials. Future efforts should focus on fundamentally improving the intrinsic tolerance of perovskite materials to moisture and oxygen. Strategies such as bulk compositional doping, quasi-2D structural regulation, and multi-cation synergistic design can be employed to enhance lattice robustness and defect tolerance while simultaneously maintaining high radiative recombination efficiency and excellent optoelectronic performance in PeLEDs. Establishing such intrinsic material stability is therefore essential for achieving long-term operational reliability in air-processed PeLEDs.

(2) Rational utilization of ambient moisture and oxygen to optimize the humidity window. Most current air-processing strategies primarily aim to suppress or eliminate the influence of moisture. However, recent studies suggest that environmental components can be constructively utilized as chemical tools. For instance, Wang et al. [50] exploited the hydrolysis of phosphonic chloride in ambient air to convert pure bromide perovskite into a Br–Cl mixed-halide perovskite, significantly broadening the operational humidity window and improving film quality. Similarly, Guo et al. [51] employed the hydrolysis of $AlBr_3$ or $SiBr_4$ to construct an in situ oxygen-bridged network on quasi-2D perovskite quantum wells, effectively "encapsulating" the quantum wells. Consequently, air-processed blue-emitting films retained stable emission color even after 2160 h of exposure. These studies demonstrate that ambient components are not merely detrimental factors but can serve as active participants in structural modulation and stability enhancement. Future research should further develop strategies that deliberately harness environmental reactions for controlled air processing.

(3) Toward fully air-processed PeLED fabrication systems. To date, most reported air-processed PeLEDs still rely on high-vacuum thermal evaporation for depositing the ETL and metal electrodes. Commonly used electron transport materials in laboratory-scale devices, such as small-molecule organics and low-work-function polymers, are highly sensitive to moisture and oxygen, leading to chemical degradation or changes in surface energy under ambient conditions. These effects deteriorate film quality and induce interfacial energy level shifts. Moreover, low-work-function metals (e.g., LiF/Al, Mg), which are widely employed as cathodes in high-performance PeLEDs, are extremely prone to oxidation and moisture-induced reactions. This results in a rapid increase in work function, poor interfacial contact, and even device failure during metal deposition. Consequently, current "air-processed" approaches remain only partially air-compatible rather than fully ambient-manufacturable. Establishing a device fabrication route in which all layers—from the bottom electrode to the top electrode—can be processed under uncontrolled atmospheric conditions represents a critical challenge for scalable manufacturing and a prerequisite for the commercial realization of PeLED technology.

Table 1. The summary of air-processed PeLEDs via dopant, antisolvent and interface engineering.

Strategy	EQE_{max} (%)	EL (nm)	Fabrication Humidity (RH)	Perovskite	Device Structure	Ref.
Bulk doping	3.02	480	≈25% RH and 20 °C	$PEA_2(CsPbBr_3)_2PbBr_4$ 15%$SbBr_3$ and 30%$GaBr_3$ relative to Pb	ITO/PVP/Perovskite/ TBPi/LiF/Al	[13]
	2.39	474		$PEA_2(CsPbBr_3)_2PbBr_4$ 10%$SbBr_3$ and 10%$GaBr_3$ relative to Pb		
	2.05	468		$PEA_2(CsPbBr_3)_2PbBr_4$ 5%$SbBr_3$ and 3%$GaBr_3$ relative to Pb		
	16.01	green	/	quasi-2D $CsPbBr_3$	ITO/Br-4PACz/PFNBr/Perovskite/ TBPi/LiF/Al	[17]
	3.3	490	25%~40%	$CsPbBr_3$	ITO/PEDOT:PSS/Perovskite/ TPBi/LiF/Al	[50]
	10.0	522	25%~40%	Ca-FACsPbBr3	ITO/2PACz/PFNBr/Perovskite/ TBPi/LiF/Al	[49]
	4.02	469	10~20%	quasi-2D $CsPbBr_3$	ITO/PVP/Perovskite/ TBPi/LiF/Al	[51]
Antisolvent engineering	15.4	525	15%~20%	quasi-2D PEA-$FAPbBr_3$ Antisolvent: diethyl ether	ITO/PEDOT:PSS/Perovskite/ TPBi/LiF/Al	[3]
	5.89	483	/	$Rb_xCs_yPbBr_zCl_{3-z}$ Antisolvent: n-hexane	ITO/NiO_x/PVP/Perovskite/ TPBi/LiF/Al	[14]
Interface modification	12.06	513	25%~40%	quasi-2D $CsPbBr_3$	ITO/2PACz/PFNBr/Perovskite/ TPPO/TPBi/LiF/Al	[4]
	16.05	535	/	$FAPbBr_3$	ITO/NiO_x/PVP/Perovskite/ TPBi/LiF/Al	[18]
	2.34	479	≈20% RH and 21 °C	$PEA_2(CsPbBr_3)_2PbBr_4$	ITO/NiO_x-PEIS/Perovskite/ TPBi/LiF/Al	[19]
	6.86	478	≈25% RH and 20 °C	$PEA_2Cs_4Pb_3Br_{12}$	ITO/PFOA-PEDOT:PSS/Perovskite/ TPBi/LiF/Al	[52]
	4.87	512	55 ± 5%	quasi-2D $CsPbBr_3$	ITO/2PACz/Perovskite/TPPO/TPBi/LiF/Al	[53]

Author Contributions

X.C.: conceptualization, investigation, formal analysis, data curation, visualization, writing—original draft; E.L.L.: conceptualization, formal analysis, data curation, supervision, funding acquisition, writing—review & editing; Z.W.: supervision, funding acquisition, validation. All authors have read and agreed to the published version of the manuscript.

Funding

We acknowledge the funding support by the National Key Research and Development Program of China (No. 2022YFA1204800), the National Natural Science Foundation of China (No. U21A2078), and the Scientific Research Funds of Huaqiao University.

Institutional Review Board Statement

Not applicable.

Informed Consent Statement

Not applicable.

Data Availability Statement

The data are available from the corresponding author on reasonable request.

Conflicts of Interest

The authors declare no conflict of interest.

Use of AI and AI-Assisted Technologies

No AI tools were utilized for this paper.

References

1. Yuan, L.; Xue, Q.; Wang, F.; et al. Perovskite Solar Cells and Light Emitting Diodes: Materials Chemistry, Device Physics and Relationship. *Chem. Rev.* **2025**, *125*, 5057–5162.
2. Cheng, Y.; Wan, H.; Sargent, E.H.; et al. Reduced-Dimensional Perovskites: Quantum Well Thickness Distribution and Optoelectronic Properties. *Adv. Mater.* **2025**, *37*, 2410633.
3. Liu, Y.; Bu, T.; Ono, L.K.; et al. Phase Aggregation Suppression of Homogeneous Perovskites Processed in Ambient Condition toward Efficient Light-Emitting Diodes. *Adv. Funct. Mater.* **2021**, *31*, 2103399.
4. Li, W.; Li, T.; Tong, Y.; et al. Reducing Nonradiative Losses of Air-Processed Perovskite Films via Interface Modification for Bright and Efficient Light Emitting Diodes. *Adv. Funct. Mater.* **2024**, *34*, 2311133.
5. Cui, Y.; Zhu, D.; Chen, J.; et al. Ion-pair pinning on perovskite quantum dots for high-efficiency air-processed light-emitting diodes with Rec. 2020 compliance. *Light Sci. Appl.* **2026**, *15*, 151.
6. Gu, X.; Zhang, X.; Ren, D.; et al. Ambient-air fabrication of perovskite solar cells: Challenges, progress, and perspectives. *Green Energy Environ.* **2026**, *11*, 359–386.
7. Do, Q.-H.; Antony, R.; Ratier, B.; et al. Improving Device-to-Device Reproducibility of Light-Emitting Diodes Based on Layered Halide Perovskites. *Electronics.* **2024**, *13*, 1039.
8. Peng, J.; Xue, X.; Liu, S.; et al. Maximizing perovskite electroluminescence with ordered 3D/2D heterojunction. *Nature.* **2026**, *651*, 76–82.
9. Jiang, J.; Xia, Z.; Shi, M.; et al. Efficient Red Perovskite LEDs with Iodine Management via Volatile Additive I(2). *Adv. Mater.* **2025**, *37*, e2503699.
10. Gao, Y.; Cai, Q.; He, Y.; et al. Highly efficient blue light-emitting diodes based on mixed-halide perovskites with reduced chlorine defects. *Sci. Adv.* **2024**, *10*, eado5645.
11. Peng, C.; Yao, H.; Ali, O.; et al. Weakly space-confined all-inorganic perovskites for light-emitting diodes. *Nature.* **2025**, *643*, 96–103.
12. Kim, J.S.; Heo, J.M.; Park, G.S.; et al. Ultra-bright, efficient and stable perovskite light-emitting diodes. *Nature.* **2022**, *611*, 688–694.
13. Guo, Y.; Yang, P.; Dong, F.; et al. Lattice Stabilized and Emission Tunable Pure-Bromide Quasi-2D Perovskite for Air-Processed Blue Light-Emitting Diodes. *Adv. Sci.* **2025**, *12*, e2414499.
14. Yang, S.; Bo, W.; Zhou, J.; et al. Regulating the interaction between perovskite precursor solution and antisolvent for

efficient air-processed blue perovskite light-emitting diodes. *Chem. Eng. J.* **2025**, *522*, 168194.
15. Li, H.; Wu, J.; Hu, S.; et al. Air-Processed Blue Perovskite Light-Emitting Diodes Enabled by Manipulation of Adsorbed-Moisture-Dominated Crystallization Kinetics. *Adv. Funct. Mater.* **2023**, *33*, 2303787.
16. Du, J.; Chen, J.; Cui, Y.; et al. Eco-Friendly and Air-Compatible Fabrication of Reduced-Dimensional Perovskites for High-Efficiency Light-Emitting Diodes. *ACS Photonics.* **2026**, *13*, 542–548.
17. Tong, Y.; Wang, Y.; Qi, H.; et al. Regulating Crystallization and Carrier Recombination of Quasi-2D Perovskite for Efficient Air-Processed Light-Emitting Diodes. *Nano Lett.* **2025**, *25*, 8834–8842.
18. Ding, J.; Yang, S.; Zhang, Y.; et al. Air-processed efficient and pure green perovskite LEDs based on a PVP-modified NiO(x) interface layer. *Chem. Commun.* **2025**, *61*, 11613–11616.
19. Wu, J.; Li, H.; Yang, Y.; et al. Bilateral Embedded Anchoring via Tailored Polymer Brush for Large-Area Air-Processed Blue Light-Emitting Diodes. *Angew. Chem. Int. Ed.* **2024**, *63*, e202411361.
20. Cheng, Y.; Chen, J.; Wu, S.; et al. Air-Processed Perovskites Enabled by an Interface-Reconstruction Strategy for High-Performance Light-Emitting Diodes. *Nano Lett.* **2025**, *25*, 6192–6199.
21. Guan, X.; Li, Y.; Meng, Y.; et al. Targeted elimination of tetravalent-Sn-induced defects for enhanced efficiency and stability in lead-free NIR-II perovskite LEDs. *Nat. Commun.* **2024**, *15*, 9913.
22. Bhatia, H.; Martin, C.; Keshavarz, M.; et al. Deciphering the Role of Water in Promoting the Optoelectronic Performance of Surface-Engineered Lead Halide Perovskite Nanocrystals. *ACS Appl. Mater. Interfaces.* **2023**, *15*, 7294–7307.
23. Yan, P.; Zhang, W.; Wang, C.; et al. Acetamidinium based 2D alternating cation perovskite for efficient solar cells. *J. Alloys Compd.* **2024**, *977*, 173298.
24. Soe, C.M.M.; Stoumpos, C.C.; Kepenekian, M.; et al. New Type of 2D Perovskites with Alternating Cations in the Interlayer Space, $(C(NH_2)_3)(CH_3NH_3)nPbnI_{3n+1}$: Structure, Properties, and Photovoltaic Performance. *J. Am. Chem. Soc.* **2017**, *139*, 16297–16309.
25. Leung, T.L.; Ahmad, I.; Syed, A.A.; et al. Stability of 2D and quasi-2D perovskite materials and devices. *Commun. Mater.* **2022**, *3*, 63.
26. Stranks, S.D.; Hoye, R.L.Z.; Di, D.; et al. The Physics of Light Emission in Halide Perovskite Devices. *Adv. Mater.* **2019**, *31*, 1803336.
27. Cheng, S.; Zhong, H. What Happens When Halide Perovskites Meet with Water? *J. Phys. Chem. Lett.* **2022**, *13*, 2281–2290.
28. Folastre, N.; Akhavan Kazemi, M.A.; Cherednichneko, K.; et al. Water-induced spinodal decomposition of mixed halide perovskite captured by real-time liquid TEM imaging. *Energy Environ. Sci.* **2024**, *17*, 8745–8755.
29. Jin, X.; Li, Z.; Wang, S.; et al. Water-Influenced Perovskite Materials: Crystal Transition, Stability Regulation, and Applications. *Adv. Opt. Mater.* **2025**, *13*, e01785.
30. Haight, G.P. Relation between solubility and solubility product is a limiting case. *J. Chem. Educ.* **1978**, *55*, 452.
31. Geng, C.; Xu, S.; Zhong, H.; et al. Aqueous Synthesis of Methylammonium Lead Halide Perovskite Nanocrystals. *Angew. Chem. Int. Ed.* **2018**, *57*, 9650–9654.
32. Wang, P.; Wang, B.; Li, N.; et al. Alkali-Metal–Assisted Green-Solvent Synthesis for In Situ Growth of Perovskite Nanocrystals in Porous Materials. *Adv. Sci.* **2024**, *11*, 2305880.
33. Wang, R.H.; Qin, R.H.; Jin, R.J.; et al. Advancing Two-Dimensional Perovskite Solar Cells: Structural Evolution, Stability Mechanism, and Heterojunction Engineering. *Small.* **2026**, *22*, e13854.
34. Wygant, B.R.; Ye, A.Z.; Dolocan, A.; et al. Probing the Degradation Chemistry and Enhanced Stability of 2D Organolead Halide Perovskites. *J. Am. Chem. Soc.* **2019**, *141*, 18170–18181.
35. Jiang, X.; Zhang, J.; Ahmad, S.; et al. Dion-Jacobson 2D-3D perovskite solar cells with improved efficiency and stability. *Nano Energy.* **2020**, *75*, 104892.
36. Wang, G.; Chu, H.; Deng, K.; et al. Metal effect boosts the photoelectric properties of two-dimentional Dion-Jacobson (3AMPY)(MA)3M4I13 perovskites. *J. Colloid Interface Sci.* **2025**, *692*, 137493.
37. Dučinskas, A.; Kim, G.Y.; Moia, D.; et al. Unravelling the Behavior of Dion–Jacobson Layered Hybrid Perovskites in Humid Environments. *ACS Energy Lett.* **2020**, *6*, 337–344.
38. Mahal, E.; Manna, S.S.; Das, S.; et al. Understanding moisture stability and degradation mechanisms of 2D hybrid perovskites: Insights from ab initio molecular dynamics simulations. *Energy Adv.* **2024**, *3*, 1992–2001.
39. Ju, Y.; Hu, X.; Wu, X.-G.; et al. The interactions between halide perovskites and oxygen: From stages to strategies. *Matter.* **2024**, *7*, 3756–3785.
40. Zou, Y.; Yu, W.; Qu, B.; et al. Ambient fabrication of perovskites for photovoltaics. *Nat. Rev. Mater.* **2025**, *10*, 400–402.
41. Shin, D.; Zu, F.; Koch, N. Reversible oxygen-induced p-doping of mixed-cation halide perovskites. *APL Materials.* **2021**, *9*, 081104.
42. Halder, A.; Itzhak, A.; Hodesh, E.R.; et al. Surface Interactions of Oxygen Suffice to P-Dope the Halide Perovskites. *Adv. Mater. Interfaces.* **2022**, *9*, 2200569.

43. Huang, L.; Ge, Z.; Zhang, X.; et al. Oxygen-induced defect-healing and photo-brightening of halide perovskite semiconductors: Science and application. *J. Mater. Chem. A.* **2021**, *9*, 4379–4414.
44. Nosaka, Y.; Nosaka, A.Y. Generation and Detection of Reactive Oxygen Species in Photocatalysis. *Chem. Rev.* **2017**, *117*, 11302–11336.
45. Wang, S.; Jiang, Y.; Juarez-Perez, E.J.; et al. Accelerated degradation of methylammonium lead iodide perovskites induced by exposure to iodine vapour. *Nature Energy.* **2016**, *2*, 16195.
46. Aristidou, N.; Sanchez-Molina, I.; Chotchuangchutchaval, T.; et al. The Role of Oxygen in the Degradation of Methylammonium Lead Trihalide Perovskite Photoactive Layers. *Angew. Chem. Int. Ed.* **2015**, *54*, 8208–8212.
47. Zhang, L.; Sit, P.H.L. Ab initio study of the role of iodine in the degradation of CH3NH3PbI3. *J. Mater. Chem. A.* **2017**, *5*, 23976–23986.
48. Na Quan, L.; Ma, D.; Zhao, Y.; et al. Edge stabilization in reduced-dimensional perovskites. *Nat. Commun.* **2020**, *11*, 170.
49. Feng, S.; Du, Q.; Liang, Y.; et al. Air-Fabrication Perovskite Supercrystal Film Enabled by a Strategy of Nontoxic Calcium Ion Confinement for Bright and Stable Light-Emitting Diodes. *Small.* **2025**, *21*, e09168.
50. Wang, H.; Qi, H.; Zhang, Z.; et al. Phosphonic Chloride Assisted Fabrication of Highly Emissive Mixed Halide Perovskite Films in Ambient Air for Blue Light-Emitting Diodes. *ACS Appl. Mater. Interfaces.* **2024**, *16*, 28771–28779.
51. Guo, Y.; Yang, P.; Dong, F.; et al. Quantum-Well Encapsulation Enabling Air-Processed Quasi-2D Perovskites with Long-Term Stability for Large-Area Deep-Blue Light-Emitting Diodes. *Adv. Funct. Mater.* **2025**, *36*, e09277.
52. Guo, Y.; Li, H.; Yang, P.; et al. Perfluorooctanoic acid interface modification enabling efficient true-blue perovskite light-emitting diodes and air-processing compatibility. *Chem. Eng. J.* **2024**, *490*, 151764.
53. Li, W.; Li, T.; Tong, Y.; et al. Fabrication of Highly Luminescent Quasi Two-Dimensional CsPbBr3 Perovskite Films in High Humidity Air for Light-Emitting Diodes. *ACS Appl. Mater. Interfaces.* **2023**, *15*, 36602–36610.
54. Hang, P.; Xie, J.; Li, G.; et al. An Interlayer with Strong Pb-Cl Bond Delivers Ultraviolet-Filter-Free, Efficient, and Photostable Perovskite Solar Cells. *iScience.* **2019**, *21*, 217–227.
55. Zia, W.; Byranvand, M.M.; Yeddu, V.; et al. Single-crystalline MAPbCl3 thin-films for photo- and X-ray voltaics. *EES Solar.* **2025**, *1*, 810–818.
56. Wei, L.; Tian, S.; Sun, M.; et al. Exploring the Critical Factors Toward Spectrally Stable Mixed-Halide Blue Perovskite LEDs. *ChemPhotoChem.* **2024**, *8*, e202400019.